

pubs.acs.org/journal/abseba Article

Integrated Biophysical Characterization of Fibrillar Collagen-Based Hydrogels

Alex Avendano, Jonathan J. Chang, Marcos G. Cortes-Medina, Aaron J. Seibel, Bitania R. Admasu, Cassandra M. Boutelle, Andrew R. Bushman, Ayush Arpit Garg, Cameron M. DeShetler, Sara L. Cole, and Jonathan W. Song*



Cite This: https://dx.doi.org/10.1021/acsbiomaterials.9b01873



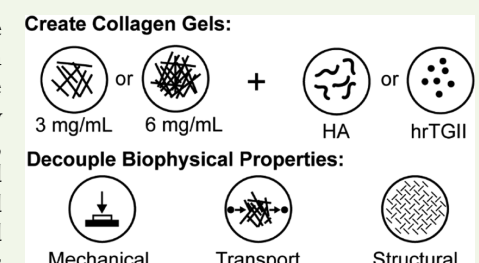
ACCESS

III Metrics & More

Article Recommendations

Supporting Information

ABSTRACT: This paper describes an experimental characterization scheme of the biophysical properties of reconstituted hydrogel matrices based on indentation testing, quantification of transport via microfluidics, and confocal reflectance microscopy analysis. While methods for characterizing hydrogels exist and are widely used, they often do not measure diffusive and convective transport concurrently, determine the relationship between microstructure and transport properties, and decouple matrix mechanics and transport properties. Our integrated approach enabled independent and quantitative measurements of the structural, mechanical, and transport properties of hydrogels in a single study. We used fibrillar type I collagen as the base matrix and investigated the effects of two different matrix modifications: (1)



cross-linking with human recombinant tissue transglutaminase II (hrTGII) and (2) supplementation with the nonfibrillar matrix constituent hyaluronic acid (HA). hrTGII modified the matrix structure and transport but not mechanical parameters. Furthermore, changes in the matrix structure due to hrTGII were seen to be dependent on the concentration of collagen. In contrast, supplementation of HA at different collagen concentrations altered the matrix microstructure and mechanical indentation behavior but not transport parameters. These experimental observations reveal the important relationship between extracellular matrix (ECM) composition and biophysical properties. The integrated techniques are versatile, robust, and accessible; and as matrix—cell interactions are instrumental for many biological processes, the methods and findings described here should be broadly applicable for characterizing hydrogel materials used for three-dimensional (3-D) tissue-engineered culture models.

KEYWORDS: extracellular matrix, mechanical behavior, collagen microstructure, transport properties, microfluidics

1. INTRODUCTION

The tissue space between living cells, commonly known as the interstitium, is comprised primarily of structural extracellular matrix (ECM) proteins and aqueous fluid. This environment is complex, information-rich, and provides cells with instructive cues to dictate emergent behavior. ECM composition has a profound influence on the biophysical properties of the interstitium.²⁻⁴ These properties include structural, mechanical, and transport, which in turn can directly or indirectly affect cell behavior and tissue-level response. 5-7 For instance, the predominant ECM protein in vivo is type I collagen, which forms a fibrillar network. The microstructural properties of the collagen network, such as mean pore size, fiber alignment, and fiber radius, are known to influence cell adhesion, proliferation, migration, and differentiation. $^{8-10}$ This collagen scaffold can be further modified by cross-linking agents such as tissue transglutaminase 2 (TGII).^{3,11,12} In addition to collagen, glycosaminoglycans (GAGs) are an important structural ECM constituent that helps provide hydrated gel-like properties of the interstitium.¹³ The collagen and GAG ECM compositions can vary greatly by tissue-type and be altered dramatically during diseased states such as cancer and fibrosis.¹⁴ These

matrix alterations impact the mechanical compliance at both the bulk and local tissue levels and their subsequent effects on fundamental cell behaviors such as morphogenesis, proliferation, motility, differentiation, and response to therapeutic agents. Mass transport properties of the interstitium also affect cell behavior by modulating shear stresses, biomolecular gradients, nutrient availability, waste clearance, and drug delivery. 17–22

While the biophysical properties of tissues can be measured in vivo, studying these properties in this setting is challenging due to limited experimental control over ECM composition. With regards to transport properties, it is very difficult to specify concentration and pressure gradients in vivo and identify the independent contributions of diffusion and convection. In response, three-dimensional (3-D) hydrogel-based culture models comprised of either synthetic or natural

Received: December 9, 2019 Accepted: February 5, 2020 Published: February 5, 2020



biomaterials have been widely adopted to provide physiological-like settings in vitro. Among the materials used to mimic the interstitial ECM, reconstituted type I collagen and the nonsulfated GAG hyaluronic acid (HA) have been used extensively due to their abundance in the interstitium, commercial availability, and versatility. The characterization of collagen hydrogel systems in terms of structure, mechanics, and transport has been accomplished in the past. Yet, these previous studies have not provided an integrated analysis of these biophysical properties of collagen-based matrices in a single study, which among other challenges make it difficult to simultaneously consider diffusive and convective transport, establish the relationship between microstructural parameters and transport efficiency, and decouple matrix mechanics and transport properties.

Detailed and systematic characterization of the biophysical properties of reconstituted acellular hydrogels is necessary to define the initial conditions for the dynamic and two-way reciprocal interactions between the matrix and cells. These findings can benefit others in studying ECM reorganization in health and disease along with its subsequent impact on cell function. Therefore, the goal of this study is to present an integrated biophysical characterization scheme using mechanical indentation testing, confocal reflectance imaging and analysis, microfluidics, and fluorescence recovery after photobleaching (FRAP) to profile structural, mechanical, and transport properties of acellular collagen-based hydrogels. This methodology has the advantages of: (1) simultaneously integrating structure, mechanical, and transport profiling in a single study, (2) independently investigating convective and diffusive transport, and (3) decoupling matrix mechanics and interstitial transport. We demonstrate the broad utility of this approach by using type I collagen as the base hydrogel scaffold and probed for the biophysical effects of matrix cross-linking by human recombinant tissue transglutaminase II (hrTGII) and addition of exogenous HA. Surprisingly, the addition of hrTGII was seen to modify the matrix structure and transport but not mechanical parameters. Furthermore, changes in the matrix structure due to hrTGII were seen to be dependent on the concentration of collagen. The supplementation of HA at different collagen concentrations altered the matrix microstructure and mechanical indentation but not transport parameters. Collectively, the results from this study demonstrate intriguing effects for these modifications made possible through the advantages enabled by the reported characterization approach.

2. MATERIALS AND METHODS

2.1. Preparation and Casting of Collagen Matrices. Polymerized collagen matrices were prepared per manufacturer's instructions. Briefly, rat-tail type I collagen stored in acidic solution (Corning Life Sciences) was neutralized to pH = 7.4 using sodium hydroxide in 10× phosphate-buffered saline. Dulbecco's modified Eagle's medium (DMEM) media was then utilized to adjust the final concentration of collagen to 3 and 6 mg/mL. Collagen gels were preincubated at 4 °C for approximately 12 min prior to casting to enhance fiber formation.²⁴ Human recombinant tissue transglutaminase II (hrTGII) (R&D Systems) was added to collagen matrices by dissolving this component (1.0 μ g) into DMEM during hydrogel preparation.²⁶ hrTGII drives a transamination reaction that produces amide cross-links between glutamine and lysine residues in collagen fibrils.²⁷ Collagen cross-linking by hrTGII was verified by primary amine group quantification with trinitrobenzene sulfonic acid,²⁷ as previously described. Hyaluronic acid (HA) salt from bovine vitreous

humor (Sigma, molecular weight (MW) \sim 400 kDa²⁸) was dissolved in DMEM and added during the casting of collagen matrices.²⁹ The incorporation of HA was verified by alcian blue staining³⁰³⁰ (Figure S1).

Upon neutralization and preincubation, collagen gels were pipetted into the different configurations used for the characterization scheme (Figure 1). For indentation testing, 300 μ L of the gel was cast in a

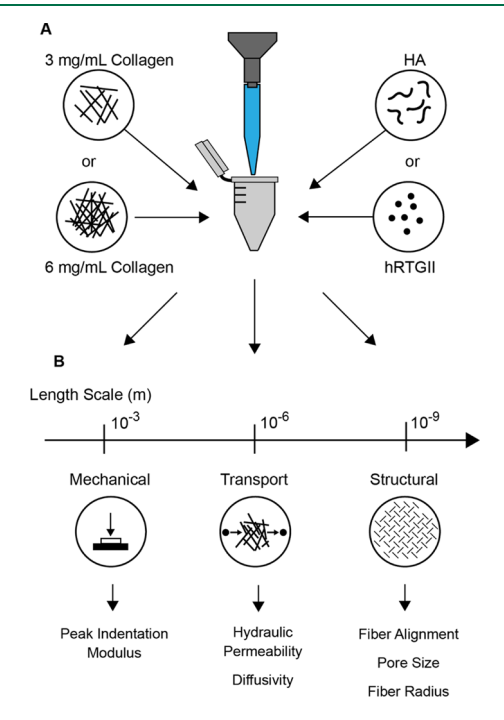


Figure 1. Integrated approach for characterizing collagen-based matrices supplemented with either hrTGII or HA. (A) Collagen gels were prepared and characterized (B) with measurements of mechanical, transport, and structural parameters across varying length scales.

cylindrical mold obtained from laser cutting a 48-well plate (Eppendorf). For mass transport measurements (i.e., hydraulic permeability and diffusivity) and confocal reflectance imaging of collagen fibers, gels were cast inside poly(dimethylsiloxane) (PDMS) microchannels bonded irreversibly to a glass coverslip. Upon casting, gels were placed in a humidified incubator at 37 $^{\circ}\text{C}$ for at least 20 min to complete polymerization before being subsequently hydrated with DMEM media. All samples were stored at 37 $^{\circ}\text{C}$ for 48 h prior to data acquisition to ensure complete polymerization and equilibrium swelling conditions. 23

2.2. Mechanical Indentation Testing and Data Analysis. The mechanical stiffness of different ECM hydrogels was represented by the peak indentation modulus, which is a measure of the resistance to peak compressive loading.³¹ Indentation testing of collagen-based matrices was conducted as previously described 31 (Figure 2A-C). Briefly, the well containing the gel was loaded into a high precision mechanical load frame (ElectroForce 5500, TA Instruments) and subjected to four incremental stress-relaxation indentations at a strain rate $(\dot{\varepsilon})$ of 10% of the gel thickness $(t_{\rm gel})$ using a metallic circular flatended indenter (Figure 2A,B). Each indentation step was performed to a depth of 10% of the sample thickness (~3 mm). Peak indentation loads were then converted to peak indentation stresses using known indenter geometry and plotted against the corresponding strain. The peak indentation modulus was then estimated by computing the slope of the peak indentation stress-strain curve produced from these measurements (Figure 2C). Post-measurement analyses were done automatically using custom scripts written in MATLAB.

2.3. Microfluidic Hydraulic Permeability Measurement. Convective transport of the collagen gels was characterized by the

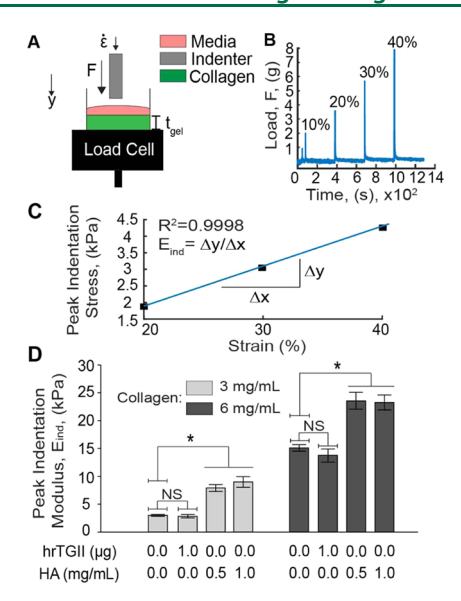


Figure 2. Quantification of the peak indentation modulus of different ECM compositions. (A) Collagen gels in cylindrical molds were loaded into a mechanical load frame and subjected to incremental indentation—relaxation steps at a strain rate $(\dot{\epsilon})$ of 10% of the gel thickness $(t_{\rm gel})$. (B) The load applied to the indenter was recorded and plotted over time to obtain the peak indentation loads. (C) The peak indentation loads were converted to peak indentation stresses and plotted against the corresponding indentation strain (starting from 20%) to compute the peak indentation modulus $(E_{\rm ind})$. (D) Peak indentation modulus measurements. hrTGII did not alter the peak indentation modulus compared to control conditions. Addition of HA significantly increased the peak indentation loading for both 3 and 6 mg/mL collagen gels.

parameter hydraulic or Darcy permeability, which determines the flow rate in a porous material under an applied pressure gradient.³² Hydraulic permeability was measured in a rectangular microfluidic device (length: 5 mm; width: 500 µm; height: 1 mm) 48 h postseeding as described in Hammer et al.³³ Briefly, a height difference across the collagen gel was created by inserting a trimmed pipet tip at one of the ports and filling the tip with the cell culture medium. This height difference produces a pressure gradient across the microchannel that generates flow through the seeded collagen type I matrix. The average velocity of the flow is estimated by tracking the motion of a fluorescent tracer dye within the microchannel (tetramethylrhodamine isothiocyanate (TRITC)-bovine serum albumin (BSA), MW = 65.5 kDa) using time-lapse microscopy. Images were recorded every 5 s for a duration of 20-30 min using a Nikon TS-100F microscope equipped with a Q-Imaging QIClick camera controlled with the NIS-Elements software. A custom MATLAB algorithm was then developed to automatically estimate the hydraulic permeability from the timelapse movies. The algorithm imports each frame and estimates the position of the dye profile by subtracting the image at t = i with the image at t = i - 1 and tracking the centroid of the resulting difference image (Figure S2). The position of the centroid is then plotted over time, and the slope is obtained to approximate the bulk dye velocity (v) (Figure 3). Darcy's law (eq 1) was then used to calculate the hydraulic permeability

hydraulic permeability =
$$\frac{\nu \times \mu \times \Delta L}{\Delta P}$$
 (1)

where μ is the viscosity of the fluid (0.001 Pa s), ΔL is the length of the microfluidic channel (5 mm), and ΔP is the hydrostatic pressure gradient across the hydrogel estimated by (eq 2)

$$\Delta P = \rho \times g \times h \tag{2}$$

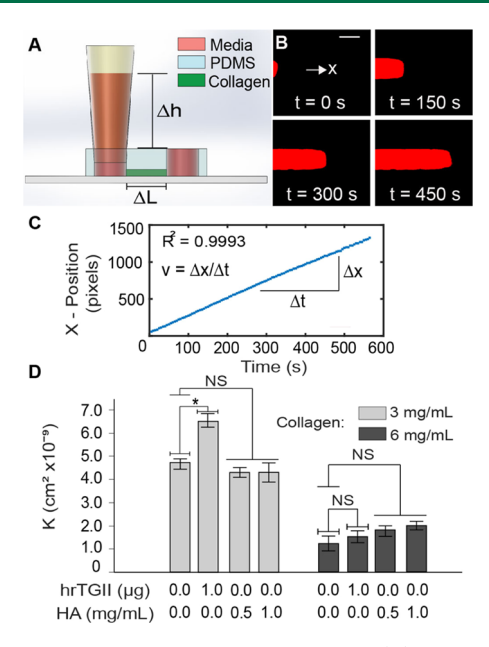


Figure 3. Hydraulic permeability measurements. (A) Straight channel PDMS devices with 4 mm ports are sealed into a glass slide or a coverslip and a trimmed pipet tip is inserted (inset) to create a pressure difference that generates flow across the channel. Collagen type I of different compositions is injected and polymerized within the microfluidic device. (B) Time-lapse microscopy is used to track BSA—TRITC dye across the channel to obtain the average velocity of the flow (C) (scale bar = 150 μ m). Darcy's law is then used to estimate the hydraulic permeability. (D) Hydraulic permeability quantification. hrTGII did increase the hydraulic permeability for 3 mg/mL collagen matrices but not for 6 mg/mL. Addition of HA did not alter the hydraulic permeability of the matrices for both collagen concentrations.

where ρ is the density of the fluid (1000 kg/m³), g is the acceleration due to gravity (9.81 m/s²), and h is the fluidic height difference between the microfluidic channel ports.

2.4. Measurement of Diffusivity in the Microfluidic Device. Quantification of matrix diffusivity to the fluorescent tracer dye (TRITC-BSA, MW = 65.5 kDa) was done with the use of fluorescence recovery after photobleaching (FRAP) on rectangular microchannels (L: 20 mm, W: 3 mm, T: 20 μ m).³⁴ FRAP measurements were conducted on an Olympus FV1000 multiphoton microscope equipped with a DeepSee MaiTai titanium-sapphire laser using a 40× water immersed objective (NA: 0.80) and an excitation wavelength of 840 nm. The laser was focused on a 40 μ m circular region of interest (ROI) for 10 s to bleach the dye followed by image acquisition at intervals of 0.243 s for a total of 14 s (Figure 4A). Diffusivities were estimated using an automated custom-made MATLAB script with a procedure previously described by Brancato et al.³⁵ Briefly, the mean intensity inside the ROI was measured and converted to normalized fractional intensity (f). This parameter was then plotted versus time and fitted with an exponential curve to determine the half-recovery time τ where f = 0.5 (Figure 4B). The diffusivity was then calculated by (eq 3)

$$diffusivity = \frac{\omega^2}{4 \times \tau}$$
(3)

where ω^2 is the radius of the bleach region (40 μ m).

2.5. Quantification of Peclet Number. The relative contributions of diffusion and convection to mass transport in matrices were quantified via the dimensionless parameter, Peclet number $(Pe)^{36}$

$$Pe = \frac{L_c v}{D} \tag{4}$$

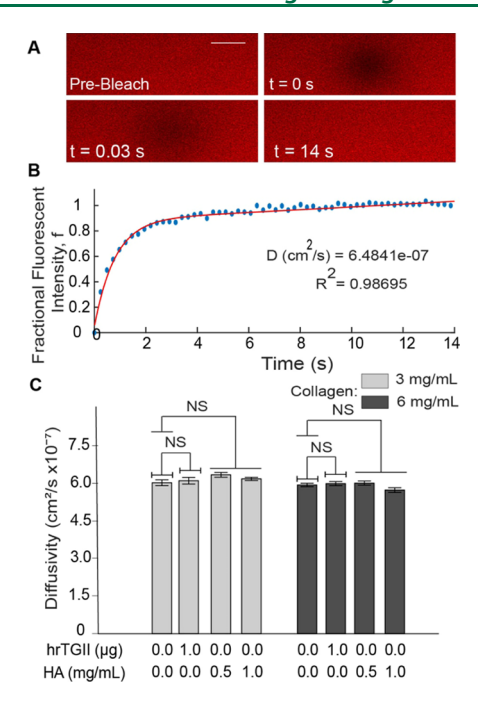


Figure 4. Interstitial diffusivity measurements with fluorescence recovery after photobleaching (FRAP). (A) Images were recorded in the collagen-based matrices in PDMS microchannels loaded with BSA–TRITC dye. A bleached circular region was created and allowed to recover over time (scale bar = 40 μ m). (B) Intensity in the bleached region is quantified over time and used to calculate the fractional fluorescent intensity. This parameter is plotted over time and fitted to estimate the diffusivity of the matrix. (C) Diffusivity quantification. Modifications to collagen matrices with hrTGII or HA did not significantly alter the diffusivity for both collagen concentrations considered.

where $L_{\rm c}$ denotes the characteristic length of interstitial transport (~100 μ m), ν denotes the fluid velocity through the matrices measured in Section 2.3 for estimating hydraulic permeability, and D denotes the matrix interstitial diffusivity.

2.6. Confocal Reflectance Microscopy Image Acquisition. Collagen fibers within the microfluidic device (Figure 5A) were imaged using confocal microscopy on a Nikon A1R live cell imaging confocal microscope via a 40×1.3 NA oil immersion lens controlled with the NIS-Elements software. The reflectance signal was detected by exciting samples with a 487 nm laser, passing the reflected light through a 40/60 beam splitter, and collecting it in a detector for visualization of collagen fibers. Tonfocal reflectance stacks of approximately $50~\mu m$ in height with a z-step of $0.59~\mu m$ were acquired for image analysis (80-90 total images per stack). In each experiment, duplicate devices were imaged for each condition. When imaging, three stacks per device were obtained. Each condition was run three to five times in independent experiments.

2.7. Collagen Fiber Image Analysis. Confocal reflectance stacks of collagen fibers were analyzed to quantify the fiber alignment, the average pore size of the matrix, and fiber radii. Collagen fiber alignment was assessed using a fast Fourier transform (FFT) analysis as described previously. Confocal reflection images of collagen fibers were converted into grayscale and analyzed for alignment using a custom-made MATLAB program. The alignment was summarized with the computation of an alignment index that indicates the degree of anisotropy of the collagen fibers by comparing intensity fractions within 20° of the most occurrent angle in the image to the same fraction in a random histogram. With this criterion, values close to 1 represent randomly aligned fibers, while values greater than 1 represent highly aligned fibers. The average pore size of the matrix was estimated by the use of the nearest obstacle distance (NOD) method. In this approach, the average pore size was quantified by

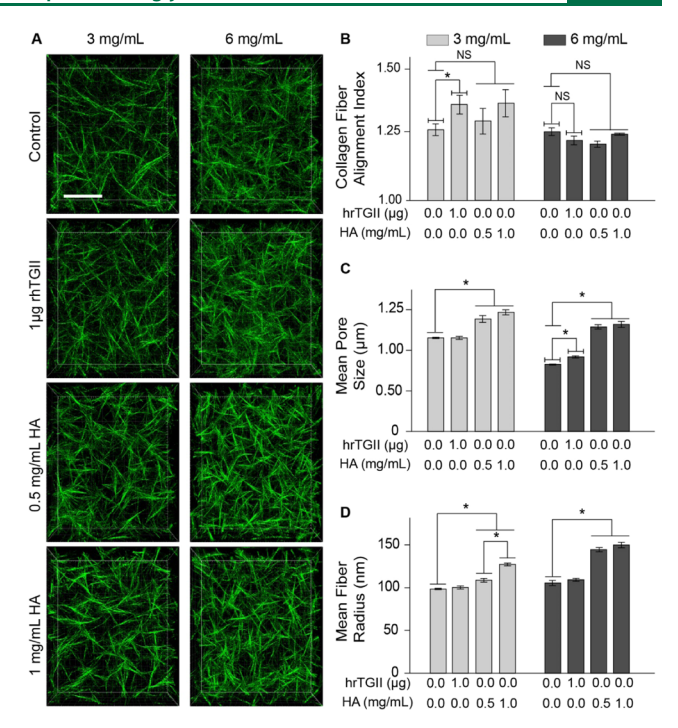


Figure 5. Microstructural characterization of collagen-based matrices. (A) Confocal projections of 3 and 6 mg/mL collagen matrices with added hrTGII and HA (scale Bar = $20~\mu m$). (B) Average matrix pore size determined by the nearest obstacle method. hrTGII did not alter the pore size of 3 mg/mL collagen matrices and slightly increased the pore size of 6 mg/mL collagen matrices. HA increased the average matrix pore size for both collagen concentrations. (C) Alignment of collagen fibers quantified with alignment index. hrTGII increased the alignment of 3 mg/mL collagen matrices but not for 6 mg/mL matrices. Addition of HA did not alter the alignment index at either collagen concentration. (D) Mean fiber radius quantified through 3-D skeletonization. Addition of HA significantly increased the radius of collagen fibers at both collagen concentrations. hrTGII did not alter the radius of the collagen fibers.

fitting a Rayleigh distribution to the Euclidian distance transform of the binarized stack to obtain the biased average pore radius of the network. This value is then corrected for missing out-of-plane fibers, assuming a cutoff angle of 43° . To quantify fiber radii, stacks were imported into FIJI and subsequently skeletonized in 3-D using the Skeleton tool. The total skeleton length was then computed and used to estimate the radius of the fibers from the known collagen concentration.

2.8. Statistical Analysis. Differences in properties of hrTGII-supplemented collagen hydrogels were compared to control matrices at each concentration with the use of a *t*-test. To evaluate the differences between control matrices and those with added HA, analysis of variance (ANOVA) was used followed by Tukey's posttesting for pairwise comparisons between collagen controls and different concentrations of HA. All data are presented with bar graphs alongside error bars representing the standard error from the mean. Each condition was characterized independently at least three times, and all data were pooled together for statistical evaluation. A *p*-value of less than 0.05 was used as a threshold for statistical significance for the differences observed between conditions.

3. RESULTS

3.1. Differential Effects of TGII and HA on Altering the Mechanical Stiffness of Collagen-Based Matrices. We first determined the bulk mechanical properties of different ECM compositions by measuring the peak indentation modulus (Figure 2). This parameter is dependent on both

fibrillar and nonfibrillar matrix components, thus providing a rationale to assess how hrTGII-mediated cross-linking of fibrils and HA modify the mechanical behavior of collagen-based matrices. In addition, hrTGII and HA have been used to manipulate cell behavior in hydrogels, but their impact on altering matrix mechanical stiffness has not been reported. For the collagen-only matrix, at 3 mg/mL, the indentation stiffness was 3.01 kPa, and at 6 mg/mL, the indentation stiffness was 14.8 kPa (Figure 2D). For some physiological context, the stiffness profile for normal breast tissue is ~3.00 kPa, ^{14,41} while the previously reported range of stiffness measurements for breast cancer tissue is 10.0–42.0 kPa. Our results demonstrate that 3 mg/mL collagen recapitulates the tissue stiffness profile for normal breast, while 6 mg/mL approximates the lower range of stiffness for breast cancer.

Next, we measured the indentation modulus of collagen that was cross-linked with hrTGII. At 3 mg/mL collagen, addition of hrTGII resulted in an indentation modulus of 2.87 kPa; at 6 mg/mL collagen, addition of hrTGII resulted in an indentation modulus of 14.3 kPa. Importantly, collagen cross-linking by hrTGII was verified by primary amine group quantification with trinitrobenzene sulfonic acid²⁷ (Figure S1). Therefore, cross-linking by hrTGII application did not significantly modify the indentation stiffness of collagen gels for both concentrations considered (Figure 2D). In contrast to hrTGII, addition of HA to the collagen gels significantly increased the peak indentation modulus for both collagen concentrations considered (Figure 2D). At 3 mg/mL of collagen, addition of HA at concentrations of 0.5 and 1.0 mg/mL significantly increased the indentation stiffness compared to collagen-only matrices to 7.92 and 9.00 kPa, respectively. At 6 mg/mL of collagen, addition of HA (0.5 and 1 mg/mL) significantly increased the indentation stiffness to ~23 kPa for both HA concentrations. Given the ability of HA to withstand compressive loading in tissues such as cartilages, 31 this increase in indentation stiffness is expected and can be attributed to HA affecting the ability of collagen fibers to reorganize in response to the applied indentation load. 42 We verified that increased HA concentration in the collagen gels resulted in increased alcian blue staining (Figure S1). Interestingly, increasing the concentration of HA from 0.5 to 1 mg/mL did not further enhance the indentation modulus, suggesting that this effect saturates beyond a certain HA concentration in collagen-based matrices.

3.2. Effects of TGII and HA on the Convective and Diffusive Transport Properties of Collagen-Based Matrices. Next, we characterized the effects of hrTGII and HA on mass transport by convection and diffusion in collagenbased matrices (Table S1). For these studies, we introduced the same ECM compositions used for the indentation testing into a single channel microfluidic device. To characterize convection through the 3-D ECM, we measured the hydraulic or Darcy permeability to fluid flow (see Section 2). Hydraulic permeability is known to be dependent on ECM structure, composition, and concentration. 43 Therefore, as expected, increasing the collagen concentration from 3 to 6 mg/mL significantly decreased the hydraulic permeability by 74% (from 4.72×10^{-9} cm² for 3 mg/mL to 1.22×10^{-9} cm² for 6 mg/mL) (Figure 3D). However, addition of hrTGII resulted in a significant increase of 38% in hydraulic permeability (from 4.72×10^{-9} to 6.51×10^{-9} cm²) compared to control at 3 mg/ mL collagen but not at 6 mg/mL concentration (Figure 3D). Interestingly, supplementation of HA to the collagen matrices

did not significantly alter the hydraulic permeability for both collagen concentrations considered (Figure 3D). At 3 mg/mL of collagen, HA addition resulted in hydraulic permeability values of $\sim\!4.30\times10^{-9}~\rm cm^2$ for both HA concentrations. At 6 mg/mL of collagen, addition of HA at 0.5 and 1 mg/mL resulted in slightly higher permeability values compared to control (1.81 \times 10 $^{-9}$ and 2.00 \times 10 $^{-9}$ cm²) but was not statistically significant.

In addition, we compared the experimental values for hydraulic permeability to multiple previously described models in literature 44-48 (Figure S3), which were derived either from phenomenological or idealized unit cell approaches. The experimental hydraulic permeability values were converted to their dimensionless form by dividing by the square of the fiber radius and plotted against the porosity of the collagen gels. Although these models follow the trend of increasing values of dimensionless permeability with increasing porosities, they tend to either overestimate or underestimate experimental values (Figure S3). Thus, caution must be exerted when applying these models in the context of collagenous gels formed at very high porosities (i.e., greater than 0.99), such as the ones used for this study. We also measured the interstitial diffusivity, which like hydraulic permeability, is dependent on ECM properties but can also depend on the size and geometry of the tracer molecule. 49 In contrast to the hydraulic permeability measurements, we observed no significant difference in the average diffusivity for all of the ECM compositions tested using FRAP-based measurements (Figure 4C). In addition, the measured values for diffusivity (\sim 6 \times 10⁻⁷ cm²/s) in our in vitro setting were comparable to previously recorded FRAP measurements in vivo $(1 \times 10^{-7} - 6)$ $\times 10^{-7}$ cm²/s). Moreover, the measured values for diffusivity of BSA collagen gels in this study were compared to theoretical diffusivity values developed for isotropic fiber networks. 50,51 The theoretical diffusivity is given by the product of hydrodynamic (F) and steric (S) interactions

$$D_{\rm gel} = D_{\rm solution} \times F \times S = D_{\rm solution} e^{a \varnothing b} e^{-0.84 f^{1.09}}$$
(5)

where $D_{\rm solution}$ is the diffusivity of BSA in solution ($\sim 6.32 \times 10^{-7}~{\rm cm^2/s}$), $^{\rm S2}$ ø is the solid fraction of the gel, f is an adjusted volume fraction given as a function of ø, and the ratio of the solute to the fiber radius (δ , $\delta = \frac{R_{\rm BSA}}{R_{\rm COL}}$, $R_{\rm BSA} \sim 3.5~{\rm nm}$ and $R_{\rm COL}$ taken from fiber radius measurements) given by $f = (1+\delta)^2$ ø. Corrected values of a and b are given as $a = \pi$ and $b = 0.174~{\rm ln}(59.6/\delta)$. The results in Table S1 confirm that the experimental data obtained with microfluidic FRAP measurements to be in good agreement with the model.

Simultaneous quantification of transport parameters within 3-D matrices enabled an estimation of the Peclet number (eq 4), which is the dimensionless ratio of convection relative to diffusion (Table S2). A Peclet number greater than 1 indicates convection-dominated transport, while a number less than 1 indicates diffusion-dominated transport. For macromolecules comparable to BSA and nanoparticles, convection is normally the dominant transport mechanism in tissues in vivo. Taking the length scale in eq 4 to be 100 μ m (or the average interstitial distance between blood vessels in normal tissues 10, the Peclet numbers were approximately 30 and 10 for 3 and 6 mg/mL collagen. Addition of hrTGII to collagen at 3 mg/mL concentration increased the Peclet number by 40% (from 30 to 42). In contrast, addition of HA had no effect on the Peclet number. Collectively, these results demonstrate that con-

vection is the dominant transport mechanism for BSA along a typical interstitial path in the reconstituted collagen-based matrices tested.

3.3. Alternations to the Collagen Matrix Microstructure by TGII and HA. Next, we assessed modifications to the collagen matrix microstructure with confocal reflectance microscopy (Figure 5A). These images were then analyzed with different image processing schemes to compute three parameters for the collagen network: (1) alignment index (dimensionless), (2) mean matrix pore size (μm) , and (3) mean fiber radius (nm). In addition, the modifications to these microstructural parameters can be correlated with the bulk mechanical (Figure 2) and transport properties (Figures 3 and 4) of the different ECM compositions. The alignment index, mean pore size, and mean fiber radius measurements for 3 mg/ mL were 1.15, 1.15 μ m, and 98.5 nm, respectively. For 6 mg/ mL, the values for these parameters were 1.23, 0.83 μ m, and 105 nm. As expected, increasing the collagen concentration from 3 to 6 mg/mL decreased the mean pore size but did not affect either the alignment or the mean fiber radius. 40,54

We then compared the effects of hrTGII and HA with collagen-only controls on matrix microarchitecture parameters. Addition of hrTGII increased the alignment of collagen fibers at 3 mg/mL by 8% (from 1.27 to 1.36) but not at 6 mg/mL collagen concentration (Figure 5B). In contrast, supplementing the collagen matrices with HA did not significantly alter the alignment of fibers for both collagen concentrations considered. For the mean matrix pore size measurements, addition of hrTGII had no effect at 3 mg/mL collagen but exhibited modest increases at 6 mg/mL (from 0.83 to 0.92 μ m) with statistical significance (Figure 5C). However, it must be noted that the estimated pore size for the collagen-only control and hrTGII-supplemented matrices at 6 mg/mL collagen lies below the resolution limit for the NOD ($\sim 1 \ \mu m$). 39,40 Therefore, the actual pore sizes for the 6 mg/mL collagen matrices may be smaller and the difference in pore sizes between the two collagen concentrations evaluated may be greater. In contrast to the hrTGII-supplemented matrices, addition of HA significantly increased the mean pore size for both 3 mg/mL (by 30%, from 1.15 to 1.39 and 1.47 μ m) and 6 mg/mL (by 57%, from 0.83 to \sim 1.30 μ m for both HA conditions) collagen concentrations. The increase in the matrix pore size may be attributed to HA-induced swelling, an effect that has been previously observed when incorporating HA in collagen gels. 55,56 Finally, for the mean fiber radius, addition of hrTGII had no effect. Conversely, addition of HA significantly increased the mean fiber radius for both 3 mg/mL (by 10-30%, from 98.5 to 109 nm (0.5 mg/mL HA) and 127 nm (1 mg/mL HA)) and 6 mg/mL (by 43%, from 105 to 148 nm for both HA conditions) collagen concentrations (Figure 5D). This outcome may be explained by previous reports of HA associating around the collagen fibers during collagen fibrillogenesis.5

4. DISCUSSION

Understanding the relationship between ECM composition and biophysical properties is necessary to help advance the utility of in vitro tissue-equivalent systems for studying cell behavior. This study puts forth a versatile, robust, and accessible experimental characterization scheme for interstitium mimicking materials based on indentation testing, quantification of transport via microfluidics, and the confocal reflectance microscopy analysis. Here, we carefully charac-

terized how hrTGII-mediated cross-linking and HA regulate the physical characteristics of reconstituted acellular collagen-based matrices. TGII was selected as a representative example of enzymatic cross-linking that is upregulated in pathologies such as idiopathic pulmonary fibrosis.³ HA was chosen as a representative example due to its prominent role in fibrotic and desmoplastic diseases.⁵⁸

Collagen cross-linking has been correlated with increases in stiffness in the context of cell-seeded matrices. For instance, it has been reported that hrTGII may indirectly modulate the stiffness of cell-seeded collagen matrices by altering cellular responses⁵⁹ such as contractility⁶⁰ that are independent of its cross-linking functions. Yet, our measurements in acellular collagen-based matrices demonstrate no modification of indentation stiffness due to cross-linking by hrTGII alone. Therefore, our results support previous findings that direct changes to the mechanical integrity of fibrous collagen scaffolds require the formation of additional cross-link products than the ones enabled by hrTGII application under the provided conditions.⁶¹ With regards to matrix transport properties, solute diffusivity was unaffected by any of the modifications considered, including hrTGII application. In contrast, hrTGII significantly increased the hydraulic permeability for 3 mg/mL collagen gels, whereas it did not modify hydraulic permeability of 6 mg/mL collagen gels. We also observed significantly increased fiber alignment due to hrTGII treatment for 3 mg/mL but not 6 mg/mL collagen gels. Thus, the alignment index computations of the collagen fibers help explain the outcomes for hydraulic permeability as fibers aligned parallel to the direction of flow confer less resistance than fibers aligned at an angle.⁶²

In contrast to hrTGII, HA (MW ~ 400 kDa) supplementation noticeably increased the measured indentation stiffness of both 3 and 6 mg/mL collagen gels. In addition, increases in the indentation stiffness for HA-supplemented matrices were correlated with the enhanced mean matrix fiber radius and the mean matrix pore size. Both of these microstructural changes to the collagen network may be a function of the size or molecular weight of the HA molecules, which in turn can impact the chemical expansion or swelling properties.⁶³ While our study did not consider resistance to indentation due to the swelling stresses conferred by HA, this parameter can be studied using more specialized testing approaches.⁶⁴ Our results for the mean fiber radius demonstrate that HA significantly increases the radii of collagen fibers for all of the collagen/HA compositions evaluated. Moreover, these results also suggest that collagen fiber reorientation to an applied peak indentation load may depend on the radius of collagen fibers.

With regards to transport properties, cell-mediated HA deposition had been correlated with decreased hydraulic permeability in cell-laden collagen hydrogels in vitro and in vivo. 33,62,65,66 However, in the context of this study, no modification to hydraulic permeability due to HA supplementation of acellular collagen matrices was observed. These results suggest that the flow reducing effects of HA on transport properties may be dependent on both its assembly and distribution in the collagen ECM. For instance, it is believed that cells assemble high-molecular-weight HA (MW > 1000 kDa) and degrade it into fragments of varying lower molecular weights (20 monosaccharides to 1000 kDa), which can impart different biological functions. Based on these criteria, we believe the HA used in this study (MW \sim 400

kDa) is more representative of low-molecular-weight HA. Previous works on collagen and HA (MW ~ 155 kDa) assembly in vitro suggest that HA associates around the collagen fibers as opposed to being distributed within the interfibrillar space, 69 thereby minimizing hindrance to the fluid flow. Since our study was in acellular matrices in vitro and using a comparable molecular weight HA, we believe that our results point to the latter scenario. Moreover, our microstructural analysis by confocal reflectance microscopy showed that HA significantly increases both the mean fiber radii and matrix pore sizes for all of the collagen/HA combinations tested. When integrating our microstructural and transport results, it appears that low-molecular-weight HA-mediated increases in the mean fiber radius and the matrix pore size are in effect neutralizing each other in terms of transport path in porous media and subsequently hydraulic permeability. Furthermore, since HA had no effect on the hydraulic permeability of collagen matrices, this result suggests that the observed increases in indentation stiffness for this ECM composition were due to collagen fiber enhancement as opposed to increased pressurization of the interstitial fluid. Finally, our results demonstrate that for both hrTGII- and HAmodified matrices, mechanical and transport properties may act independent of each other and can be used as different measures to profile tissue or tissue-equivalent constructs.

In addition to hydraulic permeability, another important transport parameter is diffusivity. Our results were that diffusivity to BSA was unaffected by any of the ECM modifications considered, even when increasing the collagen content from 3 to 6 mg/mL and the HA content from 0.5 to 1 mg/mL. This outcome suggests that at very low gel fractions, diffusive transport is unaffected when cross-linking with hrTGII or increasing the collagen and HA content within the range of concentrations considered. However, the effect on diffusivity may be more pronounced when considering higher collagen and HA concentrations than the ones used in our studies.⁶³ Our results also support the notion that the hydrogel structure does not modify the diffusion of particles with a hydrodynamic radius (~3.5 nm, BSA) significantly smaller than the pore size of the matrix $(1-1.25 \mu m)$. ⁷⁰ Given that the diffusivities for the tested matrices were comparable, changing the Peclet number of these matrices is achieved by modifying the hydraulic permeability.

For fibrillar scaffolds, establishing a relationship between transport efficiency with microstructural parameters has been challenging due to complex ECM network morphologies that can preclude straightforward measurements of transport parameters. However, this study demonstrates the utility of microfluidic devices for addressing this challenge as all of the transport measurements and microstructural analyses were done in microfluidic devices integrated with collagen-based scaffolds. Pressure gradients in microfluidic devices can be specified with relative ease for accurate hydraulic permeability measurements.³⁶ Also, the optical clarity of the materials used for microfluidic device fabrication (i.e., PDMS channels sealed against a coverglass slide) is conducive for high-resolution confocal reflectance microscopy and FRAP-based diffusion measurements. We previously leveraged microfluidic systems to assess functional changes in hydraulic permeability mediated by cancer-associated stromal fibroblasts that were perturbed biologically by either genetic manipulations or targeted pharmacological inhibitors. 33,66 Therefore, we foresee the integrated biophysical characterizations from this study to be

part of the toolkit of functional assessments used in microfluidic-based organ-on-a-chip settings that can be readily scaled-up for high-throughput screening applications.⁷¹

While this study focused on characterizing acellular type I collagen, the physical profiling scheme presented in this study can also be applied to other natural and synthetic hydrogel materials used in tissue engineering applications (e.g., fibrin, matrigel, and alginate) as well as assessing the effects of other matrix modifications during polymerization, such as temperature ramping. Moreover, future studies can be applied in cell-laden hydrogels to investigate the physical consequences due to various physiologically important cell-mediated matrix modifications, such as enzymatic degradation by matrix metalloproteinases, formation of more mature cross-links, and deposition of sulfated GAGs and other proteoglycans.

5. CONCLUSIONS

The characterization scheme presented in this study enabled new insight as to how hrTGII and HA modify the physical characteristics of reconstituted type I collagen matrices in the absence of cells. Given the widespread use of hydrogels across tissue engineering applications, another important aspect of this study is that it brings together a collection of methods that can assist others in decoupling matrix mechanics from matrix transport properties across different length scales. These advantages can be used by the biomaterial research community for biophysical profiling of interstitium mimicking materials. In addition, the results from this study can help guide future considerations of supplementing fibrous hydrogels with exogenous hrTGII and HA for tissue engineering applications by understanding the effects on structural, mechanical, and transport parameters in vitro.

ASSOCIATED CONTENT

5 Supporting Information

The Supporting Information is available free of charge at https://pubs.acs.org/doi/10.1021/acsbiomaterials.9b01873.

Modification of collagen matrices with HA and hrTGII (Figure S1); tracking of dye flow profile for measurement of hydraulic permeability (Figure S2); comparison of experimental hydraulic permeability with theoretical models (Figure S3); comparison of experimental and theoretical diffusivity to BSA (Table S1); summary of mechanical stiffness, hydraulic permeability, diffusivity, and Peclet numbers for ECM compositions (Table S2); Theoretical models used for predicting hydraulic permeability (Table S3) (PDF)

AUTHOR INFORMATION

Corresponding Author

Jonathan W. Song — Department of Mechanical and Aerospace Engineering and Comprehensive Cancer Center, The Ohio State University, Columbus, Ohio 43210, United States; orcid.org/0000-0002-6991-5298; Email: song.1069@

Authors

osu.edu

Alex Avendano — Department of Biomedical Engineering, The Ohio State University, Columbus, Ohio 43210, United States Jonathan J. Chang — Department of Biomedical Engineering, The Ohio State University, Columbus, Ohio 43210, United States

- Marcos G. Cortes-Medina Department of Biomedical Engineering, The Ohio State University, Columbus, Ohio 43210, United States
- **Aaron J. Seibel** Department of Biomedical Engineering, The Ohio State University, Columbus, Ohio 43210, United States
- Bitania R. Admasu Department of Materials Science and Engineering, The Ohio State University, Columbus, Ohio 43210, United States
- Cassandra M. Boutelle Department of Integrated Systems Engineering, The Ohio State University, Columbus, Ohio 43210, United States
- Andrew R. Bushman William G. Lowrie Department of Chemical and Biomolecular Engineering, The Ohio State University, Columbus, Ohio 43210, United States
- Ayush Arpit Garg Department of Biomedical Engineering and Department of Mechanical and Aerospace Engineering, The Ohio State University, Columbus, Ohio 43210, United States
- **Cameron M. DeShetler** St. Charles Preparatory School, Bexley, Ohio 43209, United States
- Sara L. Cole Campus Microscopy and Imaging Facility, The Ohio State University, Columbus, Ohio 43210, United States

Complete contact information is available at: https://pubs.acs.org/10.1021/acsbiomaterials.9b01873

Notes

The authors declare no competing financial interest.

ACKNOWLEDGMENTS

J.W.S. acknowledges NSF CAREER Award (CBET-1752106), The American Cancer Society (IRG-67-003-50), and The Ohio State University Materials Research Seed Grant Program, funded by the Center for Emergent Materials, an NSF-MRSEC, grant DMR-1420451, the Center for Exploration of Novel Complex Materials, and the Institute for Materials Research. A.A., J.J.C., and J.W.S. acknowledge funding from Pelotonia. M.G.C.-M. acknowledges funding from Graduate Enrichment and Discovery Scholars Fellowships from Ohio State University and from a Graduate Diversity Supplement from the National Heart, Lung, and Blood Institute (R01HL141941-02S1). Confocal reflectance microscopy images presented in this report were generated using instruments and services at the Campus Microscopy and Imaging Facility, The Ohio State University. This facility is supported in part by grant P30 CA016058, National Cancer Institute.

REFERENCES

- (1) Baker, B. M.; Chen, C. S. Deconstructing the third dimension: how 3D culture microenvironments alter cellular cues. *J. Cell Sci.* **2012**, *125*, 3015–3024.
- (2) Lee, J.; Condello, S.; Yakubov, B.; Emerson, R.; Caperell-Grant, A.; Hitomi, K.; Xie, J.; Matei, D. Tissue Transglutaminase Mediated Tumor-Stroma Interaction Promotes Pancreatic Cancer Progression. *Clin. Cancer Res.* **2015**, *21*, 4482–4493.
- (3) Philp, C. J.; Siebeke, I.; Clements, D.; Miller, S.; Habgood, A.; John, A. E.; Navaratnam, V.; Hubbard, R. B.; Jenkins, G.; Johnson, S. R. Extracellular Matrix Cross-Linking Enhances Fibroblast Growth and Protects against Matrix Proteolysis in Lung Fibrosis. *Am. J. Respir. Cell Mol. Biol.* **2018**, *58*, 594–603.
- (4) Ricard-Blum, S. The collagen family. *Cold Spring Harbor Perspect. Biol.* **2011**, 3, No. a004978.
- (5) Yao, W.; Li, Y.; Ding, G. Interstitial Fluid Flow: The Mechanical Environment of Cells and Foundation of Meridians. *Evidence-Based Complementary Altern. Med.* **2012**, 2012, No. 853516.

- (6) Wells, R. G. Tissue mechanics and fibrosis. Biochim. Biophys. Acta, Mol. Basis Dis. 2013, 1832, 884–890.
- (7) Weaver, V. M. Cell and tissue mechanics: the new cell biology frontier. *Mol. Biol. Cell* **2017**, *28*, 1815–1818.
- (8) Noriega, S. E.; Hasanova, G. I.; Schneider, M. J.; Larsen, G. F.; Subramanian, A. Effect of Fiber Diameter on the Spreading, Proliferation and Differentiation of Chondrocytes on Electrospun Chitosan Matrices. *Cells Tissues Organs* **2012**, *195*, 207–221.
- (9) Carey, S. P.; Goldblatt, Z. E.; Martin, K. E.; Romero, B.; Williams, R. M.; Reinhart-King, C. A. Local extracellular matrix alignment directs cellular protrusion dynamics and migration through Rac1 and FAK. *Integr. Biol.* **2016**, *8*, 821–835.
- (10) Murphy, C. M.; Duffy, G. P.; Schindeler, A.; O'Brien, F. J. Effect of collagen-glycosaminoglycan scaffold pore size on matrix mineralization and cellular behavior in different cell types. *J. Biomed. Mater. Res., Part A* **2016**, *104*, 291–304.
- (11) Langhans, S. A. Three-Dimensional in Vitro Cell Culture Models in Drug Discovery and Drug Repositioning. *Front. Pharmacol.* **2018**, *9*, No. 6.
- (12) Irawan, V.; Sung, T. C.; Higuchi, A.; Ikoma, T. Collagen Scaffolds in Cartilage Tissue Engineering and Relevant Approaches for Future Development. *Tissue Eng. Regener. Med.* **2018**, *15*, 673–697.
- (13) Wiig, H.; Swartz, M. A. Interstitial fluid and lymph formation and transport: physiological regulation and roles in inflammation and cancer. *Physiol. Rev.* **2012**, *92*, 1005–1060.
- (14) Cox, T. R.; Erler, J. T. Remodeling and homeostasis of the extracellular matrix: implications for fibrotic diseases and cancer. *Dis. Models Mech.* **2011**, *4*, 165–178.
- (15) McKee, C. T.; Last, J. A.; Russell, P.; Murphy, C. J. Indentation Versus Tensile Measurements of Young's Modulus for Soft Biological Tissues. *Tissue Eng.*, Part B **2011**, *17*, 155–164.
- (16) Leight, J. L.; Drain, A. P.; Weaver, V. M. Extracellular Matrix Remodeling and Stiffening Modulate Tumor Phenotype and Treatment Response. *Annu. Rev. Cancer Biol.* **2017**, *1*, 313–334.
- (17) Dolor, A.; Sampson, S. L.; Lazar, A. A.; Lotz, J. C.; Szoka, F. C.; Fields, A. J. Matrix modification for enhancing the transport properties of the human cartilage endplate to improve disc nutrition. *PLoS One* **2019**, *14*, No. e0215218.
- (18) Fan, D.; Creemers, E. E.; Kassiri, Z. Matrix as an interstitial transport system. *Circ. Res.* **2014**, *114*, 889–902.
- (19) Fleury, M. E.; Boardman, K. C.; Swartz, M. A. Autologous morphogen gradients by subtle interstitial flow and matrix interactions. *Biophys. J.* **2006**, *91*, 113–121.
- (20) Levick, J. Flow through interstitium and other fibrous matrices. Q. J. Exp. Physiol. 1987, 72, 409–437.
- (21) Swabb, E. A.; Wei, J.; Gullino, P. M. Diffusion and convection in normal and neoplastic tissues. *Cancer Res.* **1974**, *34*, 2814–2822.
- (22) Whittington, C. F.; Brandner, E.; Teo, K. Y.; Han, B.; Nauman, E.; Voytik-Harbin, S. L. Oligomers modulate interfibril branching and mass transport properties of collagen matrices. *Microsc. Microanal.* **2013**, *19*, 1323–1333.
- (23) Caliari, S. R.; Burdick, J. A. A practical guide to hydrogels for cell culture. *Nat. Methods* **2016**, *13*, 405–414.
- (24) Sung, K. E.; Su, G.; Pehlke, C.; Trier, S. M.; Eliceiri, K. W.; Keely, P. J.; Friedl, A.; Beebe, D. J. Control of 3-dimensional collagen matrix polymerization for reproducible human mammary fibroblast cell culture in microfluidic devices. *Biomaterials* **2009**, *30*, 4833–4841.
- (25) Antoine, E. E.; Vlachos, P. P.; Rylander, M. N. Review of Collagen I Hydrogels for Bioengineered Tissue Microenvironments: Characterization of Mechanics, Structure, and Transport. *Tissue Eng., Part B* **2014**, *20*, 683–696.
- (26) Fraley, S. I.; Wu, P. H.; He, L.; Feng, Y.; Krisnamurthy, R.; Longmore, G. D.; Wirtz, D. Three-dimensional matrix fiber alignment modulates cell migration and MT1-MMP utility by spatially and temporally directing protrusions. *Sci. Rep.* **2015**, *5*, No. 14580.
- (27) Orban, J. M.; Wilson, L. B.; Kofroth, J. A.; El-Kurdi, M. S.; Maul, T. M.; Vorp, D. A. Crosslinking of collagen gels by transglutaminase. *J. Biomed. Mater. Res.* **2004**, *68A*, 756–762.

- (28) Shiedlin, A.; Bigelow, R.; Christopher, W.; Arbabi, S.; Yang, L.; Maier, R. V.; Wainwright, N.; Childs, A.; Miller, R. J. Evaluation of Hyaluronan from Different Sources: *Streptococcus zooepidemicus*, Rooster Comb, Bovine Vitreous, and Human Umbilical Cord. *Biomacromolecules* **2004**, *5*, 2122–2127.
- (29) Kreger, S. T.; Voytik-Harbin, S. L., Hyaluronan concentration within a 3D collagen matrix modulates matrix viscoelasticity, but not fibroblast response. *Matrix Biol.* **2009**, *28*, 336–346 DOI: 10.1016/j.matbio.2009.05.001.
- (30) Sapudom, J.; Ullm, F.; Martin, S.; Kalbitzer, L.; Naab, J.; Moller, S.; Schnabelrauch, M.; Anderegg, U.; Schmidt, S.; Pompe, T. Molecular weight specific impact of soluble and immobilized hyaluronan on CD44 expressing melanoma cells in 3D collagen matrices. *Acta Biomater.* **2017**, *50*, 259–270.
- (31) Lake, S. P.; Hald, E. S.; Barocas, V. H. Collagen-agarose co-gels as a model for collagen-matrix interaction in soft tissues subjected to indentation. *I. Biomed. Mater. Res., Part A* **2011**, 99, 507–515.
- (32) Swartz, M. A.; Fleury, M. E. Interstitial Flow and Its Effects in Soft Tissues. *Annu. Rev. Biomed. Eng.* **2007**, *9*, 229–256.
- (33) Hammer, A. M.; Sizemore, G. M.; Shukla, V. C.; Avendano, A.; Sizemore, S. T.; Chang, J. J.; Kladney, R. D.; Cuitino, M. C.; Thies, K. A.; Verfurth, Q.; Chakravarti, A.; Yee, L. D.; Leone, G.; Song, J. W.; Ghadiali, S. N.; Ostrowski, M. C. Stromal PDGFR-alpha Activation Enhances Matrix Stiffness, Impedes Mammary Ductal Development, and Accelerates Tumor Growth. *Neoplasia* 2017, 19, 496–508.
- (34) Chary, S. R.; Jain, R. K. Analysis of Diffusive and Convective Recovery of Fluorescence after Photobleaching—Effect of Uniform Flow Field. *Chem. Eng. Commun.* **1987**, *55*, 235–249.
- (35) Brancato, V.; Gioiella, F.; Imparato, G.; Guarnieri, D.; Urciuolo, F.; Netti, P. A. 3D breast cancer microtissue reveals the role of tumor microenvironment on the transport and efficacy of free-doxorubicin in vitro. *Acta Biomater.* **2018**, *75*, 200–212.
- (36) Avendano, A.; Cortes-Medina, M.; Song, J. W. Application of 3-D Microfluidic Models for Studying Mass Transport Properties of the Tumor Interstitial Matrix. *Front. Bioeng. Biotechnol.* **2019**, *7*, No. 6.
- (37) Brightman, A. O.; Rajwa, B. P.; Sturgis, J. E.; McCallister, M. E.; Robinson, J. P.; Voytik-Harbin, S. L. Time-lapse confocal reflection microscopy of collagen fibrillogenesis and extracellular matrix assembly in vitro. *Biopolymers* **2000**, *54*, 222–234.
- (38) Ng, C. P.; Swartz, M. A. Mechanisms of interstitial flow-induced remodeling of fibroblast—collagen cultures. *Ann. Biomed. Eng.* **2006**, *34*, 446–454.
- (39) Lang, N. R.; Munster, S.; Metzner, C.; Krauss, P.; Schurmann, S.; Lange, J.; Aifantis, K. E.; Friedrich, O.; Fabry, B. Estimating the 3D pore size distribution of biopolymer networks from directionally biased data. *Biophys. J.* **2013**, *105*, 1967–1975.
- (40) Hall, M. S.; Alisafaei, F.; Ban, E.; Feng, X.; Hui, C.-Y.; Shenoy, V. B.; Wu, M. Fibrous nonlinear elasticity enables positive mechanical feedback between cells and ECMs. *Proc. Natl. Acad. Sci. U.S.A.* **2016**, *113*, 14043–14048.
- (41) Stylianopoulos, T. The Solid Mechanics of Cancer and Strategies for Improved Therapy. *J. Biomech. Eng.* **2017**, 139, No. 021004.
- (42) Lake, S. P.; Barocas, V. H. Mechanics and kinematics of soft tissue under indentation are determined by the degree of initial collagen fiber alignment. *J. Mech. Behav. Biomed. Mater.* **2012**, *13*, 25–35.
- (43) Cross, V. L.; Zheng, Y.; Choi, N. W.; Verbridge, S. S.; Sutermaster, B. A.; Bonassar, L. J.; Fischbach, C.; Stroock, A. D. Dense type I collagen matrices that support cellular remodeling and microfabrication for studies of tumor angiogenesis and vasculogenesis in vitro. *Biomaterials* **2010**, *31*, 8596–8607.
- (44) Happel, J. Viscous flow relative to arrays of cylinders. *AIChE J.* **1959**, *5*, 174–177.
- (45) Davies, C. N. The Separation of Airborne Dust and Particles. *Proc. Inst. Mech. Eng.* 1953, 167, 185–213.
- (46) Shou, D.; Fan, J.; Ding, F. Hydraulic permeability of fibrous porous media. *Int. J. Heat Mass Transfer* **2011**, *54*, 4009–4018.

- (47) Jackson, G. W.; James, D. F. The permeability of fibrous porous media. *Can. J. Chem. Eng.* **1986**, *64*, 364–374.
- (48) Kyan, C. P.; Wasan, D. T.; Kintner, R. C. Flow of Single-Phase Fluids through Fibrous Beds. *Ind. Eng. Chem. Fundam.* **1970**, *9*, 596–603
- (49) Stylianopoulos, T.; Poh, M. Z.; Insin, N.; Bawendi, M. G.; Fukumura, D.; Munn, L. L.; Jain, R. K. Diffusion of particles in the extracellular matrix: the effect of repulsive electrostatic interactions. *Biophys. J.* **2010**, *99*, 1342–1349.
- (50) Phillips, R. J. A Hydrodynamic Model for Hindered Diffusion of Proteins and Micelles in Hydrogels. *Biophys. J.* **2000**, *79*, 3350–3353.
- (51) Stylianopoulos, T.; Diop-Frimpong, B.; Munn, L. L.; Jain, R. K. Diffusion Anisotropy in Collagen Gels and Tumors: The Effect of Fiber Network Orientation. *Biophys. J.* **2010**, *99*, 3119–3128.
- (52) Gaigalas, A. K.; Hubbard, J. B.; McCurley, M.; Woo, S. Diffusion of bovine serum albumin in aqueous solutions. *J. Phys. Chem. A.* **1992**, *96*, 2355–2359.
- (53) Dewhirst, M. W.; Secomb, T. W. Transport of drugs from blood vessels to tumour tissue. *Nat. Rev. Cancer* **2017**, *17*, 738–750.
- (54) Harjanto, D.; Maffei, J. S.; Zaman, M. H., Quantitative Analysis of the Effect of Cancer Invasiveness and Collagen Concentration on 3D Matrix Remodeling. *PLoS One* **2011**, *6*, e24891 DOI: 10.1371/journal.pone.0024891.
- (55) DuFort, C. C.; DelGiorno, K. E.; Carlson, M. A.; Osgood, R. J.; Zhao, C.; Huang, Z.; Thompson, C. B.; Connor, R. J.; Thanos, C. D.; Brockenbrough, J. S.; et al. Interstitial pressure in pancreatic ductal adenocarcinoma is dominated by a gel-fluid phase. *Biophys. J.* **2016**, *110*, 2106–2119.
- (56) Lai, V. K.; Nedrelow, D. S.; Lake, S. P.; Kim, B.; Weiss, E. M.; Tranquillo, R. T.; Barocas, V. H. Swelling of Collagen-Hyaluronic Acid Co-Gels: An In Vitro Residual Stress Model. *Ann. Biomed. Eng.* **2016**, *44*, 2984–2993.
- (57) Xin, X.; Borzacchiello, A.; Netti, P. A.; Ambrosio, L.; Nicolais, L. Hyaluronic-acid-based semi-interpenetrating materials. *J. Biomater. Sci., Polym. Ed.* **2004**, *15*, 1223–1236.
- (58) Chanmee, T.; Ontong, P.; Itano, N., Hyaluronan: A modulator of the tumor microenvironment. *Cancer Lett.* **2016**, 375, 20–30 DOI: 10.1016/j.canlet.2016.02.031.
- (59) Hapach, L. A.; VanderBurgh, J. A.; Miller, J. P.; Reinhart-King, C. A. Manipulation of in vitro collagen matrix architecture for scaffolds of improved physiological relevance. *Phys. Biol.* **2015**, *12*, No. 061002.
- (60) Steppan, J.; Bergman, Y.; Viegas, K.; Armstrong, D.; Tan, S.; Wang, H.; Melucci, S.; Hori, D.; Park, S. Y.; Barreto, S. F.; Isak, A.; Jandu, S.; Flavahan, N.; Butlin, M.; An, S. S.; Avolio, A.; Berkowitz, D. E.; Halushka, M. K.; Santhanam, L. Tissue Transglutaminase Modulates Vascular Stiffness and Function Through Crosslinking-Dependent and Crosslinking-Independent Functions. *J. Am. Heart Assoc.* 2017, 6, No. e004161.
- (61) Halloran, D. O.; Grad, S.; Stoddart, M.; Dockery, P.; Alini, M.; Pandit, A. S. An injectable cross-linked scaffold for nucleus pulposus regeneration. *Biomaterials* **2008**, *29*, 438–447.
- (62) Ng, C. P.; Swartz, M. A. Fibroblast alignment under interstitial fluid flow using a novel 3-D tissue culture model. *Am. J. Physiol.: Heart Circ. Physiol.* **2003**, 284, H1771—H1777.
- (63) Erikson, A.; Andersen, H. N.; Naess, S. N.; Sikorski, P.; Davies Cde, L. Physical and chemical modifications of collagen gels: impact on diffusion. *Biopolymers* **2008**, *89*, 135–143.
- (64) Voutouri, C.; Polydorou, C.; Papageorgis, P.; Gkretsi, V.; Stylianopoulos, T. Hyaluronan-Derived Swelling of Solid Tumors, the Contribution of Collagen and Cancer Cells, and Implications for Cancer Therapy. *Neoplasia* **2016**, *18*, 732–741.
- (65) Mpekris, F.; Papageorgis, P.; Polydorou, C.; Voutouri, C.; Kalli, M.; Pirentis, A. P.; Stylianopoulos, T. Sonic-hedgehog pathway inhibition normalizes desmoplastic tumor microenvironment to improve chemo- and nanotherapy. *J. Controlled Release* **2017**, *261*, 105–112.

- (66) Pitarresi, J. R.; Liu, X.; Avendano, A.; Thies, K. A.; Sizemore, G. M.; Hammer, A. M.; Hildreth, B. E., 3rd; Wang, D. J.; Steck, S. A.; Donohue, S.; Cuitino, M. C.; Kladney, R. D.; Mace, T. A.; Chang, J. J.; Ennis, C. S.; Li, H.; Reeves, R. H.; Blackshaw, S.; Zhang, J.; Yu, L.; Fernandez, S. A.; Frankel, W. L.; Bloomston, M.; Rosol, T. J.; Lesinski, G. B.; Konieczny, S. F.; Guttridge, D. C.; Rustgi, A. K.; Leone, G.; Song, J. W.; Wu, J.; Ostrowski, M. C. Disruption of stromal hedgehog signaling initiates RNF5-mediated proteasomal degradation of PTEN and accelerates pancreatic tumor growth. *Life Sci Alliance* 2018, 1, No. e201800190.
- (67) Pluen, A.; Boucher, Y.; Ramanujan, S.; McKee, T. D.; Gohongi, T.; di Tomaso, E.; Brown, E. B.; Izumi, Y.; Campbell, R. B.; Berk, D. A.; Jain, R. K. Role of tumor-host interactions in interstitial diffusion of macromolecules: cranial vs. subcutaneous tumors. *Proc. Natl. Acad. Sci. U.S.A.* **2001**, *98*, 4628–4633.
- (68) Cyphert, J. M.; Trempus, C. S.; Garantziotis, S. Size Matters: Molecular Weight Specificity of Hyaluronan Effects in Cell Biology. *Int. J. Cell Biol.* **2015**, 2015, No. 563818.
- (69) Erikson, A.; Andersen, H. N.; Naess, S. N.; Sikorski, P.; Davies, C. d. L., Physical and chemical modifications of collagen gels: Impact on diffusion. *Biopolymers* **2008**, *89*, 135–143 DOI: 10.1002/bip.20874.
- (70) Antoine, E. E.; Vlachos, P. P.; Rylander, M. N. Tunable collagen I hydrogels for engineered physiological tissue microenvironments. *PLoS One* **2015**, *10*, No. e0122500.
- (71) Huh, D.; Hamilton, G. A.; Ingber, D. E. From 3D cell culture to organs-on-chips. *Trends Cell Biol.* **2011**, *21*, 745–754.